2014

Mapping the Operation of the Miniature Combustion Aerosol Standard (Mini-CAST) Soot Generator

Richard H. Moore
NASA Postdoctoral Program, NASA Langley Research Center, Hampton, Virginia, USA

Luke D. Ziemba
NASA Langley Research Center, Hampton, Virginia, USA

Dabrina Dutcher
Department of Chemical Engineering, Bucknell University, Lewisburg, Pennsylvania, USA

Andreas J. Beyersdorf
NASA Langley Research Center, Hampton, Virginia, USA

Kevin Chan
NASA Langley Research Center, Hampton, Virginia, USA

See next page for additional authors

Aerosol Science and Technology, 48:467–479, 2014

ISSN: 0278-6826 print / 1521-7388 online
DOI: 10.1080/02786826.2014.890694

Mapping the Operation of the Miniature Combustion Aerosol Standard (Mini-CAST) Soot Generator

Richard H. Moore,[1,2] Luke D. Ziemba,[2] Dabrina Dutcher,[3] Andreas J. Beyersdorf,[2] Kevin Chan,[2] Suzanne Crumeyrolle,[1,2] Timothy M. Raymond,[3] Kenneth L. Thornhill,[2,4] Edward L. Winstead,[2,4] and Bruce E. Anderson[2]

[1]*NASA Postdoctoral Program, NASA Langley Research Center, Hampton, Virginia, USA*
[2]*NASA Langley Research Center, Hampton, Virginia, USA*
[3]*Department of Chemical Engineering, Bucknell University, Lewisburg, Pennsylvania, USA*
[4]*Science Systems and Applications, Inc., Hampton, Virginia, USA*

The Jing Ltd. miniature combustion aerosol standard (Mini-CAST) soot generator is a portable, commercially available burner that is widely used for laboratory measurements of soot processes. While many studies have used the Mini-CAST to generate soot with known size, concentration, and organic carbon fraction under a single or few conditions, there has been no systematic study of the burner operation over a wide range of operating conditions. Here, we present a comprehensive characterization of the microphysical, chemical, morphological, and hygroscopic properties of Mini-CAST soot over the full range of oxidation air and mixing N_2 flow rates. Very fuel-rich and fuel-lean flame conditions are found to produce organic-dominated soot with mode diameters of 10–60 nm, and the highest particle number concentrations are produced under fuel-rich conditions. The lowest organic fraction and largest diameter soot (70–130 nm) occur under slightly fuel-lean conditions. Moving from fuel-rich to fuel-lean conditions also increases the O:C ratio of the soot coatings from ∼0.05 to ∼0.25, which causes a small fraction of the particles to act as cloud condensation nuclei near the Kelvin limit ($\kappa \sim 0$–10^{-3}). Comparison of these property ranges to those reported in the literature for aircraft and diesel engine soots indicates that the Mini-CAST soot is similar to real-world primary soot particles, which lends itself to a variety of process-based soot studies. The trends in soot properties uncovered here will guide selection of burner operating conditions to achieve optimum soot properties that are most relevant to such studies.

1. INTRODUCTION

Soot particles emitted by combustion processes have been shown to be second only to carbon dioxide in terms of climatic importance (Jacobson 2001; Bond et al. 2013) and induce deleterious human health impacts upon inhalation (Kumfer and Kennedy 2007; Janssen et al. 2011). Here, we use the term "soot" as a qualitative description of combustion particles, which include thermally defined elemental carbon (EC) and organic carbon (OC), as well as optically defined black carbon (BC; Petzold et al. 2013). Much work in the past several decades has focused on elucidating the properties of soot in the atmosphere and the mechanisms for its processing and removal. These efforts are complicated by the fact that the properties of freshly emitted soot are highly source dependent, and that these particles coagulate or can become quickly coated by semi-volatile species as exhaust plumes cool and mix with ambient air. These processes quickly dissociate the soot from its source, and for that reason it often is easier to focus on specific, operationally defined components of the combustion-derived aerosol, such as EC, OC, and BC.

A wide variety of thermal, incandescence, optical, and mass spectral-based techniques have been developed, which typically each measure only one of these components. Consequently, combining different measurement types enables real-time characterization of combustion-derived atmospheric aerosols. For this to happen, though, it is necessary to compare, calibrate, and validate instrument responses using a standard reference soot, whose properties are stable and well known (Cross et al. 2010; Baumgardner et al. 2012). To address this need, a number of soots and soot surrogates (e.g., carbon black, fullerene soot, and Aquadag) are commercially available, and continuous soot production can be achieved via spark discharge or by using different burner and fuel combinations. Each have their advantages and disadvantages in terms of portability, ease of use, and representative properties, and there is no single reference material that lends itself for calibration and testing of analytical instrumentation. Baumgardner et al. (2012) discuss the applicability of a number of potential soot reference materials to different light absorption, laser incandescence, and

Received 4 June 2013; accepted 9 December 2013.
Address correspondence to Richard H. Moore, NASA Langley Research Center, 8 Lindbergh Way, Hampton, VA 30332, USA. E-mail: richard.h.moore@nasa.gov
Color versions of one or more of the figures in the article can be found online at www.tandfonline.com/uast.

thermo-optical characterization techniques. While consensus has been reached on calibration standards for some techniques (e.g., fullerene soot for the single-particle soot photometer), they stress the importance of developing standards for use in instrument calibration, validation, and inter-comparison.

A promising method for soot generation is the Jing Ltd. miniature combustion aerosol standard (Mini-CAST) burner, which is a portable burner that generates soot in an N_2-quenched, laminar diffusion flame. Operation is safe, stable, and capable of generating high concentrations of soot (Jing 1999). Consequently, a large number of studies have used the Mini-CAST (or a similar, larger CAST) burner to study coated or uncoated soot in terms of optical properties, ice nucleation, and cloud droplet nucleation (Möhler et al. 2005; Schnaiter et al. 2006; Crawford et al. 2011; Henning et al. 2012). Typically, a few burner conditions are used to create soot of varying OC:EC ratios, which are well characterized. However, to date, there has not been a comprehensive study examining the soot properties and their repeatability over the full range of Mini-CAST operating conditions.

The goal of this work is three-fold. First, we characterize the microphysical, chemical, morphological, and hygroscopic properties of Mini-CAST soot over the range of operating conditions. Second, we quantify the uncertainty and reproducibility of these measurements in a laboratory setting and over a period of several months in order to assess the capability of the Mini-CAST to serve as a soot standard. Third, we compare the properties of Mini-CAST soot to those previously reported in the literature for real-world, combustion aerosols from aircraft and diesel engines.

2. MINI-CAST DESCRIPTION

A schematic of the Jing Ltd. real soot generator (RSG) Mini-CAST (Model 4202, Zollikofen BE, Switzerland; Jing 1999) is shown in the upper-left portion of Figure 1. The burner is a co-flow, laminar diffusion flame, consisting of a coaxial inner tube (10 mm diameter) containing the fuel gas stream and an outer tube (30 mm diameter) containing the dry, particle-free oxidant air stream. The flame is quenched with dry nitrogen at a height of 40 mm above the base of the combustion chamber, which freezes the combustion process and prevents oxidation of the soot particles formed near the flame front. The competition between soot formation and oxidation is explained using a simplified numerical model, as discussed in the supplementary information (SI). The soot concentration is then rapidly diluted with dry, particle-free air to inhibit particle coagulation. Soot concentration and properties can be varied by changing the flow rates of fuel (Q_{fuel}), oxidant (Q_{oxi}), and N_2 mix (Q_{mix}) gases, which affect the chemistry and temperature of the flame.

3. EXPERIMENTAL METHODS

Figure 1 shows the complete experimental setup used to assess the Mini-CAST performance. Gas streams into the burner are controlled with a series of mass flow controllers. For all experiments, the propane fuel gas flow rate (0.06 L min^{-1}), N_2 quench gas flow rate (7.5 L min^{-1}), and dilution air flow rate (20 L min^{-1}) are held constant at standard values described in the instrument manual, while varying both the flow rates of oxidation air (0.5–2.5 L min^{-1}) and N_2 mixing gas (0–0.45 L min^{-1}) over the range of operating conditions. The domain of examined flow rates is shown in Figure 2. On the left edge of this domain (i.e., $Q_{\text{oxi}} \sim 0.60$–1.0 L min^{-1} for $Q_{\text{mix}} = 0.00$–0.40 L min^{-1}), the flame was observed to extinguish due to insufficient oxygen, while a stable flame was maintained at all other operating conditions.

The soot stream is exhausted at atmospheric pressure (1013 hPa), and two sample streams are drawn continuously via a pump and critical flow orifices: one that passes through a 350°C catalytic stripper similar to Swanson and Kittelson (2010) and a bypass line. A three-way valve is used to select either the denuded or undenuded sample stream for further analysis, and the soot is drawn into an eductor operating with compressed particle-free air. All figures and data in this article refer to the undenuded soot except for a limited number of EC/OC tests that are discussed in Section 4.2. An electrically actuated

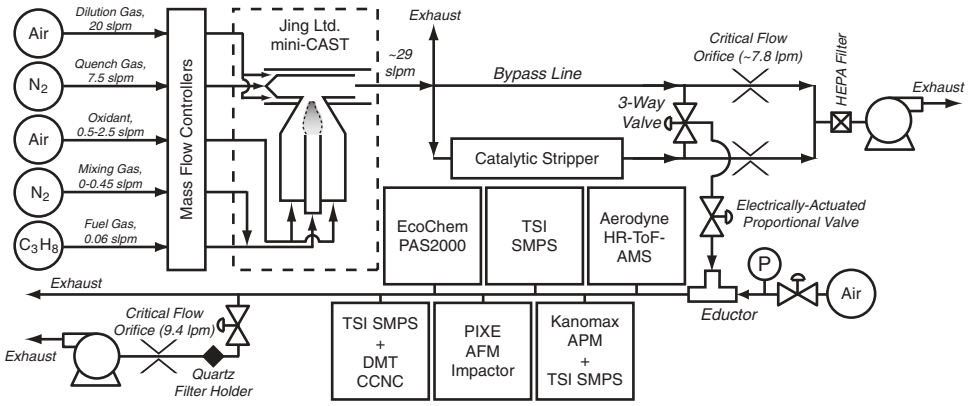

FIG. 1. Schematic of the Jing Ltd. Mini-CAST and experimental setup.

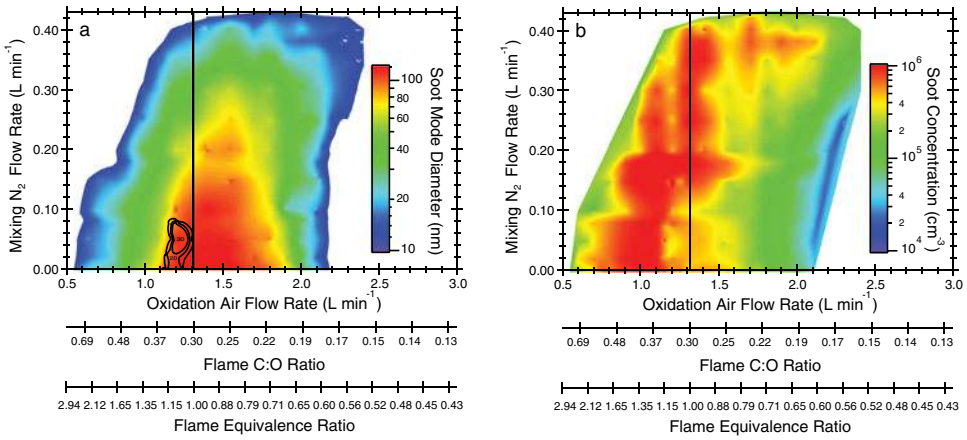

FIG. 2. (a) Soot mode diameter and (b) soot concentration over the range of Mini-CAST operation. Concentrations have not been corrected for the 172:1 (v/v) eductor dilution or for coagulation in the sample lines. The inset contours in (a) denote a region of bimodality, with the smaller modal diameter given by the contours (10–30 nm). The vertical line represents the stoichiometric flow ratio, and conditions to the left of this line are fuel-rich, while those to the right are fuel-lean.

proportional valve is used to meter the flow into the eductor and thereby increase or decrease the soot number concentration. The volumetric dilution ratio of the eductor:sample streams is maintained at 172:1 for the size and concentration measurements. Using the proportional valve was found to be more effective in controlling the soot concentration than altering the eductor flow rate, since the latter would induce pressure fluctuations. However, during long periods of operation (on the order of several hours to days), accumulation of soot within the valve was observed to cause the soot concentration to be unstable and taper off with time. Stable concentrations were restored by cleaning the valve with compressed air. The diluted soot stream is then sent to a comprehensive suite of instrumentation measuring the aerosol chemical and microphysical properties.

3.1. Size Distribution and Morphology Measurements

Size distribution measurements are made with a TSI Scanning Mobility Particle Sizer (SMPS), which consists of a long-column Differential Mobility Analyzer (DMA, TSI 3080) and a butanol-based condensation particle counter (CPC, TSI 3776) (TSI, Inc., Minneapolis, MN, USA). The SMPS is operated with a 9:1.5 sheath-to-aerosol flow ratio, and the measured size distributions are fit to two lognormal functions in order to determine the aerosol mode size and total concentration.

Additionally, we combine the SMPS with a Kanomax Aerosol Particle Mass Analyzer (APM, Model 3601; Kanomax USA, Andover, NJ, USA) to determine soot particle density. The APM consists of two concentric rotating cylinders across which a high-voltage potential is applied. The particle stream passes between the two cylinders, and a narrow range of particles whose mass-to-charge balances the centrifugal and electrostatic forces is able to exit the column, while those whose mass-to-charge is either too large or too small are lost to the cylinder walls. The classified particle stream is then sent to the SMPS, which measures the aerosol size distribution. The effective density of the particles, ρ_{eff}, is then determined as

$$\rho_{\text{eff}} = \frac{6m_{\text{p}}}{\pi D_{\text{m}}^3}, \qquad [1]$$

where m_{p} is the particle mass determined from the center of the APM transfer function and D_{m} is the particle mobility diameter determined from the center of the SMPS distribution peak. For spherical particles, ρ_{eff} is the material density of the particle; however, for aspherical particles ρ_{eff} incorporates both the material density of the particle and its morphology. For soot agglomerates, the mass-mobility exponent, x, is a useful tool for representing how the particle morphology deviates from sphericity (Schmidt-Ott et al. 1990; Park et al. 2003; Sorensen 2011):

$$\rho_{\text{eff}} = CD_{\text{m}}^{x-3}, \quad x \geq 2, \qquad [2]$$

where C is an empirical fit constant. For a homogenous, spherical particle, $x = 3$ and density does not vary with particle size.

Soot particle morphology is also characterized using a Veeco Multimode V Atomic Force Microscope (AFM; Veeco, Plainview, NY, USA) with a NanoScope V controller that was run in tapping mode. BudgetSensors Tap 190Al-G, aluminum reflex-coated tips with a nominal force constant of 48 N m^{-1} were used for all images. The particles were collected on freshly cleaved mica substrates using the smallest stage of a PIXE cascade impactor.

3.2. Chemical Composition Measurements

Soot coating chemistry is assessed with an Aerodyne high-resolution, time-of-flight, aerosol mass spectrometer (HR-ToF-AMS; Aerodyne Research, Inc., Billerica, MA, USA), operated in V-mode (Jayne et al. 2000; DeCarlo et al. 2006). The HR-ToF-AMS operates by focusing the aerosol stream onto a conical heater to vaporize the non-refractory aerosol components, which are then ionized via 70 eV electron impaction

and detected with a high-resolution, time-of-flight mass spectrometer. Since only the non-refractory aerosol components are vaporized at 600°C, this technique is not able to detect the refractory, carbonaceous soot cores. Consequently, the mass spectral information obtained from the HR-ToF-AMS applies only to the organic soot coatings. While not directly applicable to propane-derived Mini-CAST soot, the HR-ToF-AMS is also able to detect sulfate species that are commonly found in real-world combustion particles.

Soot coating chemistry is also probed using an EcoChem Analytics Photoelectric Aerosol Sensor (PAS2000; EcoChem Analytics, League City, TX, USA), which detects particle-bound polycyclic aromatic hydrocarbons (PAHs) on the soot surface. This is accomplished using an excimer UV lamp to photoionize the soot particles that are then collected on an electrically insulated filter. Measuring the electric current across the filter gives an estimate of the PAH concentration in the particles, since only PAHs can be photoionized easily. Here, we apply the universal calibration curve developed by Wall (1996), which suggests a 1:1 relationship between the PAS2000 response in pA s m^{-3} to particulate PAH in ng m^{-3} for combustion particles from a variety of real-world sources.

Total soot chemical composition, including refractory carbon, is measured using a Sunset Laboratory thermal/optical OC-EC Aerosol Analyzer (TC analyzer; Sunset Laboratory, Hillsborough, NC, USA). Quartz filters were baked at 900°C for 3 h in order to vaporize any contaminants before being used to sample soot particles from the Mini-CAST. Samples are then obtained from the polydisperse soot stream over a period of 1–20 min to obtain sufficient aerosol mass for analysis, as determined by visible discoloration of the quartz filter (typical total carbon (TC) loadings on the order of 0.5–5 μg cm^{-2}). The TC analyzer measures the amount of OC deposited on the filter by gradually heating the sample in an oxygen-free, helium carrier gas to 700°C over a period of 9 min. OC volatilizes from the filter surface and is quantified as methane using a flame ionization detector (FID) following catalytic reduction. The sample is then cooled and a mixed oxygen–helium carrier gas is introduced. The sample is gradually reheated to 910°C over a 5 min period, and the EC remaining on the filter gasifies, is catalytically reduced, and is detected by the FID. The optical transmittance of the filter is monitored during this process since it is known that some of the OC can pyrolize to form EC during the first temperature ramp, thereby decreasing the filter transmittance. Consequently, the OC/EC split point is defined as the point where the filter transmittance equals its initial transmittance. The combination of OC and EC constitutes the TC mass. The TC analyzer procedure employed here is the NIOSH He4-700 method, and a detailed discussion of this method is given by Subramanian et al. (2006).

3.3. CCN Activity Measurements

Measurements of soot hygroscopicity and cloud condensation nucleus (CCN) activity are carried out using a Droplet Measurement Technologies Stream-wise, Thermal-Gradient CCN Counter (CCNC; Droplet Measurement Technologies, Boulder, CO, USA; Roberts and Nenes 2005; Lance et al. 2006), employing Scanning Mobility CCN Analysis (SMCA; Moore et al. 2010). The CCNC exposes aerosol particles to a constant water vapor supersaturation and counts and sizes the fraction of particles that are able to nucleate cloud droplets under these conditions. The ability of a particle to act as a CCN depends on its size and chemical composition (i.e., hygroscopicity). SMCA involves coupling the CCNC to an SMPS in order to constrain particle size, and therefore, quantify the particle hygroscopicity. Mini-CAST soot did not act as CCN at atmospherically relevant supersaturations (<1%), so we pushed the upper bound of the typical CCNC operating conditions in order to activate the soot particles. To achieve this, the total instrument flow rate is held constant at 1.0 L min^{-1} and the applied temperature gradient is varied, stepwise, between 18°C and 24°C to produce a water vapor supersaturation (s) range of 2.54%–3.59%. As discussed by Moore et al. (2010), the ratio of the CCN to total aerosol distributions results in a sigmoidally shaped CCN activation curve, where the inflection point of the sigmoid corresponds to the so-called "critical activation diameter" (D_c), above which the particles act as CCN. Petters and Kreidenweis (2007), and many publications since, have combined D_c with s to compute a particle hygroscopicity (κ), which captures the compositional dependence of CCN activation.

In addition to inferences related to the CCN-active fraction of aerosols, we can use the sigmoidal activation curves to determine the externally mixed, non-CCN-active aerosol fraction. If all particles act as CCN, the upper plateau of the activation curve is unity, as all particles much greater than D_c act as CCN. In the presence of an externally mixed, non-CCN-active aerosol fraction, the upper plateau stabilizes at a value less than unity. Thus, from size-resolved CCN measurements, we can assess both the hygroscopic properties of the CCN-active fraction and its total contribution to the overall aerosol population.

4. RESULTS AND DISCUSSION

4.1. Soot Size and Concentration

Measurements of the soot size distribution were made with the SMPS at varying Q_{oxi} and Q_{mix}, and the distributions were typically found to be monomodal with mode diameters ranging from less than 10 to 130 nm. Figure 2a shows interpolated contours of these mode diameters based on data points collected at over 200 different burner flow conditions. When describing flame chemistry, it is useful to speak in terms of the overall fuel/air flame equivalence ratio, ϕ, which is shown on the lower axis of Figure 2:

$$\phi = \frac{m_{fuel}/m_{air}}{(m_{fuel}/m_{air})_{st}}, \quad [3]$$

where m_{fuel} and m_{air} are the fuel and air mass flows, respectively, and the subscript "st" denotes the stoichiometric flow ratio.

Thus, the flame is fuel-rich when $\phi > 1$ and fuel-lean when $\phi < 1$, and it can be observed from Figure 2a that the largest soot mode diameters occur under slightly fuel-lean flame conditions. Under slightly fuel-rich conditions, a second, nucleation size mode is apparent, which is much smaller ($D_{mode} \sim$ 10–30 nm) than the main soot mode ($D_{mode} \sim$ 80–100 nm), and, as will be discussed in Section 4.2, likely consists of condensed organic species rather than soot. While this nucleation mode may exist under other conditions, it is only clearly discernible from the main soot mode within the black, contoured region.

Integrating the particle size distributions yields the total number concentrations shown in Figure 2b. The reported concentrations have not been corrected for the eductor dilution (172:1, v/v) or for coagulation in the ~3 m sample lines upstream of the dilutor (estimated residence time of 6 s). The coagulation process is driven by both the aerosol number concentration and the amount of time that the aerosol stream exists in high concentration prior to dilution. For the experimental setup shown in Figure 1, the dilution is effectively constant throughout the experiment and should not depend on variations of Q_{oxi} and Q_{mix}, while the rate of particle coagulation will vary with the soot concentration leaving the burner. Consequently, the size modes and concentrations reported here may differ from results obtained with other experimental setups. This is particularly true for studies that employ a stagnation chamber to enhance coagulation and grow the soot agglomerates to large sizes (Schnaiter et al. 2006; Crawford et al. 2011). Schnaiter et al. (2006) characterized a CAST burner and observed modal diameters of 300–340 nm for $Q_{mix} = 0.0$ L min^{-1} and flame C:O ~0.25–0.29. The size mode decreased with increasing C:O ratio to less than 40 nm for the highest C:O ratio they examined of 1.0. Barthazy et al. (2006) also examined a CAST burner and uncovered a soot mode diameter of ~160 nm for $Q_{oxi} = 1.5$ L min^{-1}, which decreased to <20 nm and ~130 nm for Q_{oxi} of 0.65 and 2.0 L min^{-1}, respectively.

Here, the highest soot concentrations are found under fuel-rich flame conditions. The overall soot volume can be computed from the SMPS number size distribution by accounting for the aggregate non-sphericity as in Lall and Friedlander (2006), assuming a soot primary particle diameter of 20 nm (Mamakos et al. 2013). This soot volume is shown to correlate well with the bulk adiabatic flame temperature from chemical equilibrium calculations when the soot size exceeds 30 nm diameter (Figure 3). The highest adiabatic flame temperatures correspond to $Q_{oxi} = 1.3$ L min^{-1} ($\phi = 1$) and $Q_{mix} = 0.0$ L min^{-1}, where both concentration and particle size are near their local maxima. Moving away from this point along the Q_{mix} axis in Figure 2 keeps the flame stoichiometry constant, while decreasing the flame temperature. The result is smaller, more numerous particles, but an overall decrease in particle volume. Moving along the Q_{oxi} axis also results in smaller particles in either direction, but an increase in number toward fuel-rich conditions and a decrease toward fuel-lean conditions. Given these trends, we can parameterize the volumetric production of Mini-CAST soot, to first order, in terms of the adiabatic flame temperature

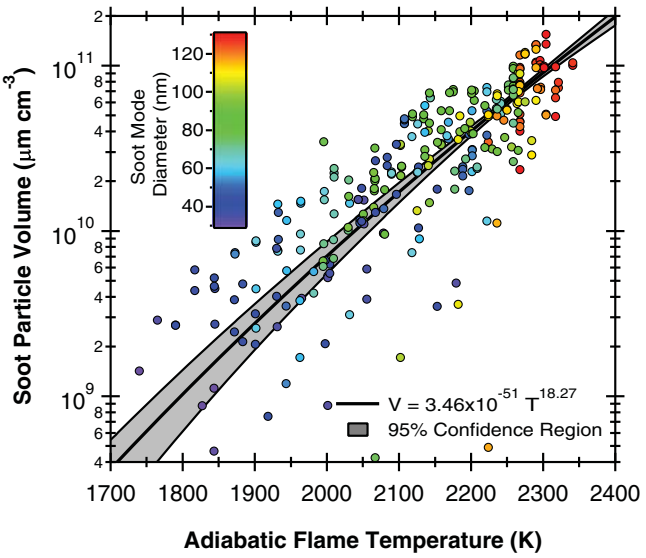

FIG. 3. Correlation between measured soot volume and adiabatic flame temperature computed using inlet flow rates. The volumes have not been corrected for the 172:1 (v/v) eductor dilution or for coagulation in the sample lines.

with higher flame temperatures producing more soot, by volume (Figure 3). This dependence makes sense because both soot formation and oxidation processes scale with the flame temperature. However, since the Mini-CAST suppresses the oxidation region by rapidly quenching the flame, it follows that soot production should monotonically increase with increasing flame temperature.

4.2. Soot Chemical Composition

Measurements of OC and EC indicate that OC mass fraction scales primarily with the soot size distribution modal diameter (Figure 4a) and is otherwise independent of flame condition. This is shown in Figure 4b, where OC/TC ratios are plotted versus Q_{oxi} for constant size contours in Figure 2a. This finding conflicts with the results of Barthazy et al. (2006), who studied soot produced by an earlier CAST model and found that the soot OC fraction was greatest at low Q_{oxi} and decreased with increasing Q_{oxi}. They attributed the decrease in OC/TC to increased oxidation of the soot prior to leaving the burner. Other studies have used CAST and Mini-CAST soot of varying OC fraction to study the impact of soot chemistry on ice nucleation or optical properties. Often these results are reported in terms of the overall flame fuel/air C:O ratio. For example, Schnaiter et al. (2006) report OC/TC ratios less than 10% for flame C:O ratios of 0.25–0.30, which increases with increasing C:O to ~80% for flame C:O ratios about 0.8–1.0. They observe the same bimodal size distribution reported here in Figure 2, and attribute the increased OC fraction to the presence of these nucleation mode particles. Crawford et al. (2011) extended the CAST data of Schnaiter et al. (2006) by looking at the OC fraction of Mini-CAST soot under similar conditions. They find a shift in OC/TC compared with the CAST burner, with OC fractions of ~30% and ~70%–80%

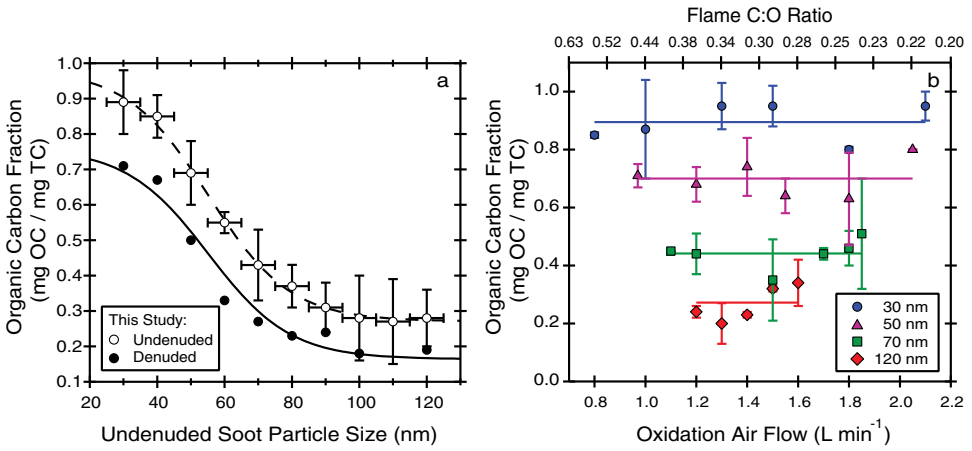

FIG. 4. Organic carbon fraction as a function of (a) particle size and (b) oxidation air flow rate along constant size contours shown in Figure 2. Vertical error bars denote the standard deviation of at least three filter samples, while the horizontal error bars reflect the uncertainty in the DMA transfer function. Denuded soots were treated with a catalytic stripper at 350° prior to sampling. These data and those from other studies are plotted as a function of flame C:O ratio in the SI.

for flame C:O ratios of 0.3 and 0.4, respectively. Mamakos et al. (2013) report OC/TC ratios for both denuded and undenuded Mini-CAST 5200 soot, and find an undenuded soot organic fraction of ~77% for C:O = 0.44 (Q_{oxi} = 1.00 L min^{-1} and Q_{mix} = 0.00 L min^{-1}), which is higher than in the present study (SI). As shown in Figure 4b, the introduction of nitrogen into the fuel stream can significantly alter both the soot mode size and OC/TC ratio, while keeping the overall flame C:O ratio constant. Marsh et al. (2011) also found that the soot OC/TC varies with both overall flame C:O ratio and Q_{mix}. This dual dependency makes it difficult to directly compare the current OC/TC data with previous studies. However, since the soot mode size and OC/TC both seem to scale with Q_{oxi} (i.e., flame C:O ratio) and Q_{mix} (Figure 4b), OC/TC collapses neatly into a monotonic curve when plotted versus soot modal size (Figure 4a). Since we neglect the influence of particle coagulation on the soot modal diameter, this relationship may not hold under conditions where coagulation processes significantly alter the soot size distribution (e.g., when using a mixing volume as in Crawford et al. 2011). Consequently, relationships based on Q_{oxi} and Q_{mix} should be used.

The high organic content of the soot has the potential to alter the light scattering, hygroscopic properties, and health impacts of the particles by coating the EC soot cores. Therefore, understanding the chemical composition of this organic fraction is important. In particular, PAHs are known from flame combustion studies to be precursors to soot inception and formation within the flame (Warnatz et al. 2001), and could be expected to be a large contributor to the organic fraction of particles from a quenched flame. Measurements of the PAH content of Mini-CAST soot were conducted with an EcoChem PAS2000 at the over 200 flame conditions used to create Figure 2, and the PAH mass to soot volume ratio is shown in Figure 5. Fitted curves to the Q_{mix} = 0.0 L min^{-1} and 0.4 L min^{-1} conditions are included to guide the eye. The PAH fraction is greatest for fuel-rich conditions (recall that $\phi = 1$ for Q_{oxi} = 1.3 L min^{-1}), with a greater than 10-fold decrease in PAH fraction as the oxidation air flow rate is increased to fuel-lean flame conditions. Increasing Q_{mix} is found to also increase the PAH fraction, but to a lesser extent than its dependence on Q_{oxi}.

Since the TC analyzer measurements indicate that the soot OC fraction is similar for Q_{mix} = 0.0 L min^{-1} and Q_{oxi} of 1.0 and 2.0 L min^{-1} (~70% from Figure 4), the observed difference in PAH fraction between these conditions suggests that the aromatics and PAHs are oxidized in the fuel-lean flame to more functionalized species. Analysis of the HR-ToF-AMS mass spectra supports this hypothesis, as shown in Figure 6. Soot organic coating O:C and H:C ratios, as well as the

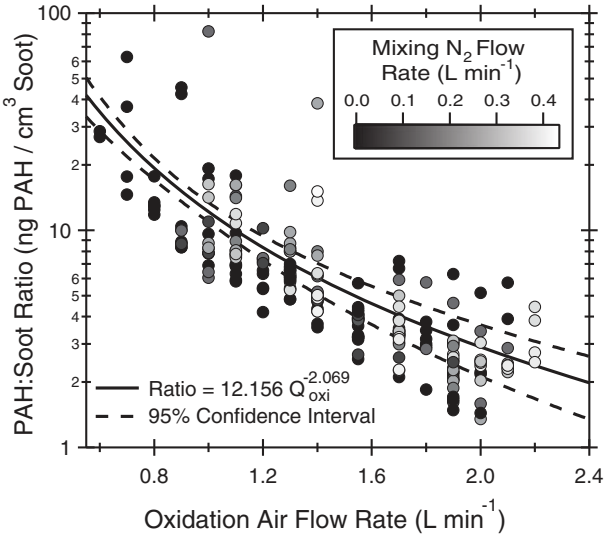

FIG. 5. PAH mass concentration measured by the EcoChem 2000 normalized by the total soot volume concentration from the SMPS. The PAH mass is derived using the universal calibration curve of Wall (1996), which suggests a 1:1 relationship between the PAS response in pA s m^{-3} and PAH in ng m^{-3}.

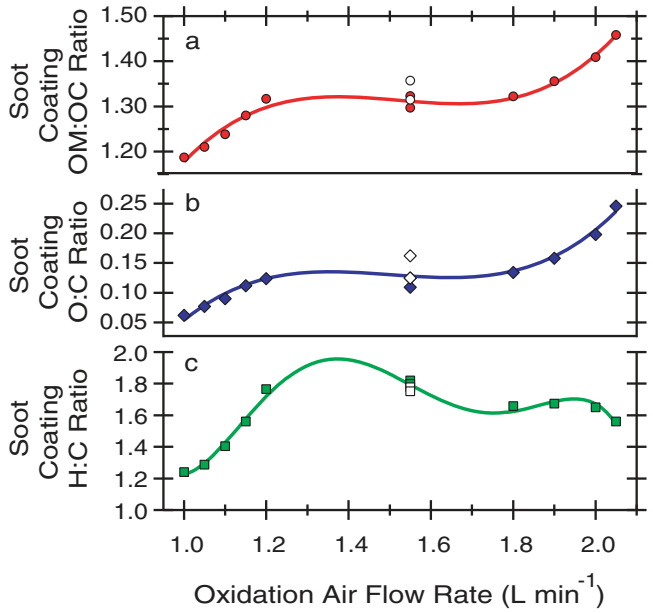

FIG. 6. The oxidation state of the soot coating over a range of Mini-CAST burner conditions as determined by the HR-ToF-AMS. $Q_{\mathrm{mix}} = 0.0$ L min^{-1} for all solid markers, while open markers denote $Q_{\mathrm{mix}} = 0.15$ and 0.30 L min^{-1}.

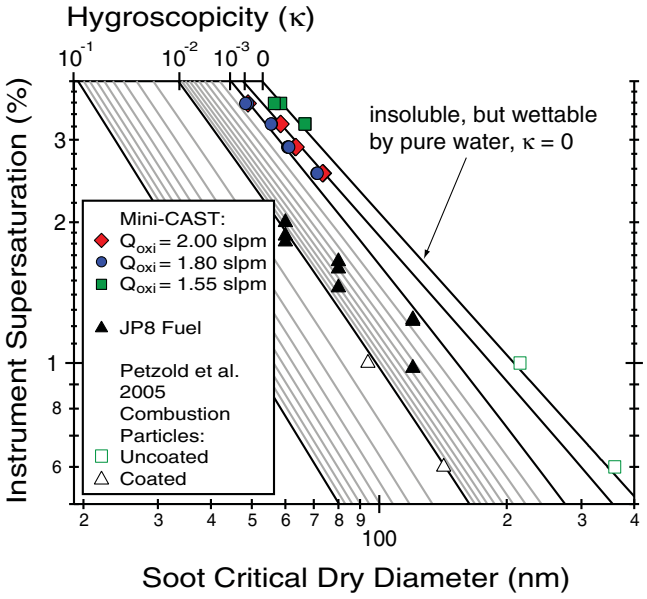

FIG. 7. CCN-derived critical supersaturation–diameter relationship for multiple Mini-CAST soot conditions. Data are overlaid on the hygroscopicity matrix of Petters and Kreidenweis (2007). Shown for comparison are unpublished CCN activity data for soot produced by a Honeywell auxiliary power unit burning JP8 jet fuel as well as coated and uncoated combustion particles reported by Petzold et al. (2005). $Q_{\mathrm{mix}} = 0.00$ L min^{-1} for all conditions.

ratio of organic matter to organic carbon (OM:OC) were computed from the mass spectra following Aiken et al. (2007) and Aiken et al. (2008). Here, OC reflects only the organic carbon mass, while OM also incorporates other atoms such as O, H, and N.

It can be seen that the soot coating O:C ratio increases by five-fold as Q_{oxi} is increased from fuel-rich to fuel-lean flame conditions. Smaller increases are seen for both the H:C and OM:OC ratios. The low H:C ratio (~1.2–1.4) under fuel-rich conditions suggests that the soot coating has a high degree of aromaticity, consistent with the PAH measurements with the PAS2000 (since H:C $\leq$ 1 for aromatics and 2 $<$ H:C $\leq$ 3 for aliphatic hydrocarbons). Changing Q_{mix} does not appear to have a substantial effect on the coating degree of oxygenation.

4.3. Soot Hygroscopicity

Figure 7 shows the CCNC instrument supersaturation plotted versus soot critical dry activation diameter for $Q_{\mathrm{oxi}} = 1.55$, 1.80, and 2.00 L min^{-1} and $Q_{\mathrm{mix}} = 0.0$ L min^{-1}. Measurements were also made at $Q_{\mathrm{oxi}} = 1.0$ and 1.2 L min^{-1}, although no particles were CCN-active. It can be observed from Figure 7 that the soot under these conditions is non-hygroscopic and behaves as a wettable, but insoluble solid ($\kappa \sim 0$). Increasing the soot coating O:C ratio results in a very slight, but noticeable, increase in the hygroscopicity (κ) of the soot (from $\kappa = 0$ to 10^{-3}). We interpret these findings such that both the soot core and surface-bound PAHs are hydrophobic; however, increased oxidation/functionalization at lower flame C:O ratios does make the surface-bound organics slightly more hydrophilic, which allows these particles to uptake water and act as CCN. Critical s-D_c pairs are also plotted for soot emissions sampled from a small, auxiliary power unit burning JP-8 jet fuel at 10 m distance downwind. The JP-8 fuel soot is more hygroscopic and acts as CCN at supersaturations below 2%, which is likely driven by the higher sulfur content of the jet fuel. It is worth noting that all soot measurements fall on the low end of the hygroscopicity spectrum, and typical atmospheric aerosols have $\kappa \sim 0.1$–0.6, which is many orders of magnitude greater than the hygroscopicities measured here (Petters and Kreidenweis 2007).

Not all of the Mini-CAST soot acts as CCN, as shown in Figure 8. The CCN-active soot fraction is greatest at all supersaturations for the most fuel-lean flame conditions and decreases to zero below $Q_{\mathrm{oxi}} = 1.5$ L min^{-1}. This finding is consistent with the increase in the PAH content of the soot found at fuel-rich flame conditions (Figure 5), since PAHs are known to have very low or no solubility in water.

These results are consistent with past studies that failed to find sub-saturated hygroscopic growth or supersaturated CCN activation ($s \leq 1\%$) for uncoated Mini-CAST soot (Friedman et al. 2011; Henning et al. 2012). Popovicheva et al. (2008) used a gravimetric method to measure sub-saturated water uptake on CAST burner soot at two conditions: flame C/O ratio of 0.29 (4% OC) and 0.4 (27% OC), which are the same conditions examined by Möhler et al. (2005). They find that more monolayers of water adsorb on the surface of the higher-OC soot than the lower-OC soot, which leads them to classify the former soot as hydrophilic

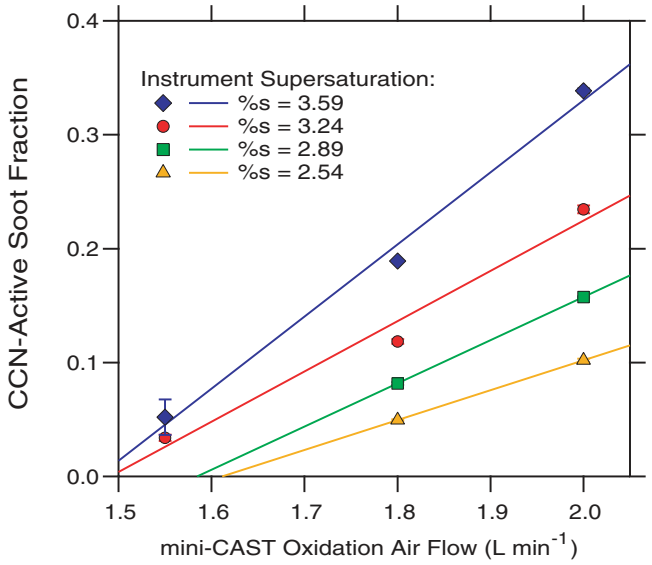

FIG. 8. CCN-active soot fraction at multiple supersaturations and Mini-CAST operating conditions. $Q_{mix} = 0.0$ L min^{-1} for all conditions.

and the latter soot as hydrophobic. Soot from an aircraft engine combustor was found to adsorb many more water monolayers at RH $< 90\%$, and this soot was classified as hygroscopic. Fourier transform infrared spectroscopy (FTIR) analysis of the lower-OC CAST soot revealed only carbonyl functional groups, while polyaromatics, carbonyl, carboxyl, and hydroxyl groups were found on the higher-OC CAST soot and on the combustor soot (Popovicheva et al. 2008). Thus, the increased water uptake was attributed to the presence of these more-polar, functionalized compounds.

Barthazy et al. (2006) and Barthazy et al. (2007) measured CAST soot hygroscopicity by measuring the soot number concentration using both a butanol-based CPC and a water-based CPC. CPCs operate by condensing the working fluid onto aerosol particles in a high-supersaturation environment that is on the order of a few percent, and then counting the number of droplets that pass through a laser beam. Condensational growth from butanol is effectively independent of the particle composition, while water uptake depends weakly on the particle composition. Thus, any differences between the two counters can be attributed to a change in particle hygroscopicity. In the first study, the flow rate of propane was varied, while keeping the flame C/O ratio constant at 0.6, and it was observed that the two CPCs were in agreement for $Q_{fuel} \leq 0.055$ L min^{-1}. The water-based CPC undercounted the butanol-based CPC by approximately two-fold at propane flow rates above that threshold (Barthazy et al. 2006). In the later study, the burner conditions were the same as in this study with $Q_{mix} = 0.0$ L min^{-1} and Q_{oxi} varied between 0.6 and 2 L min^{-1}. Here, no particles were detected by the water-based CPC for $Q_{oxi} \leq 1.5$ L min^{-1}, and the concentrations agreed within 20% above that threshold (Barthazy et al. 2007). These results are consistent with those in Figure 8, where no soot particles were found to act as CCN for $Q_{oxi} \leq 1.5$ L min^{-1}.

4.4. Soot Morphology and Effective Density

Mini-CAST soot effective densities were measured with the APM and are shown in Figure 9. Soot produced by fuel-rich flames have a much greater effective density than that produced by fuel-lean flames, while the addition of mixing N_2 to the fuel stream has only a small effect on the density. It was shown in Section 4.2 that very fuel-rich or fuel-lean flames produce soot that is mainly composed of OC with a lower degree of oxygenation and higher PAH content when $\phi > 1$ than when $\phi < 1$. A higher OC fraction soot particle would be expected to be more spherical and of higher density, since the liquid-like organic would envelope the agglomerate structure of the EC core, and this is borne out by the high soot effective density for $Q_{oxi} < 1.2$ L min^{-1}. However, the low effective density of the equally high OC soot at $Q_{oxi} > 1.8$ L min^{-1} suggests a highly non-spherical soot, which may occur through increased oxidation and volatilization of the soot coating in the fuel-lean flame. Indeed, effective density measurements of fuel-rich soot that is thermally denuded in a catalytic stripper show much lower effective densities than found for similar conditions in this study (dashed line in Figure 9). This lends support to the idea that the semi-volatile OC species fill in the gaps of the irregular non-volatile EC backbone, which yields a higher effective density than would be observed for the EC backbone alone.

Single-particle analysis with the AFM supports this conclusion, as shown in Figure 10. The three, large agglomerates shown were selected in order to clearly show the large-scale particle arrangement and morphology. In addition to the agglomerates, smaller spherical particles (~20–40 nm) were also commonly observed. The particle images in Figure 10 show the transition from higher-density, organic-dominated particles in fuel-rich flame conditions to more clearly discernible primary particles under slightly fuel-lean conditions. At the highest Q_{oxi}, particles exhibit both large organic globules combined with smaller spherules, consistent with the organic-rich, but less-dense morphology suggested by the polydisperse APM and EC:OC measurements. The height profiles in Figure 10 were used to quantify the primary particle sizes using Gaussian fits, and the peak full width at half maximum (FWHM) is reported beside each peak. The smallest particles observed under fuel-lean conditions suggest that the primary particle sizes of the EC portion of the soot are on the order of 25–30 nm, which is consistent with the upper range of primary particle size inferred by Mamakos et al. (2013). Larger peak diameters likely result from the presence of OC-coated EC agglomerates.

4.5. Size and Concentration Repeatability

To test the stability of the Mini-CAST burner over time, measurements of soot modal size and concentration were performed with the SMPS over a period of months and the results are shown in Figure 11. As before, soot concentration is computed

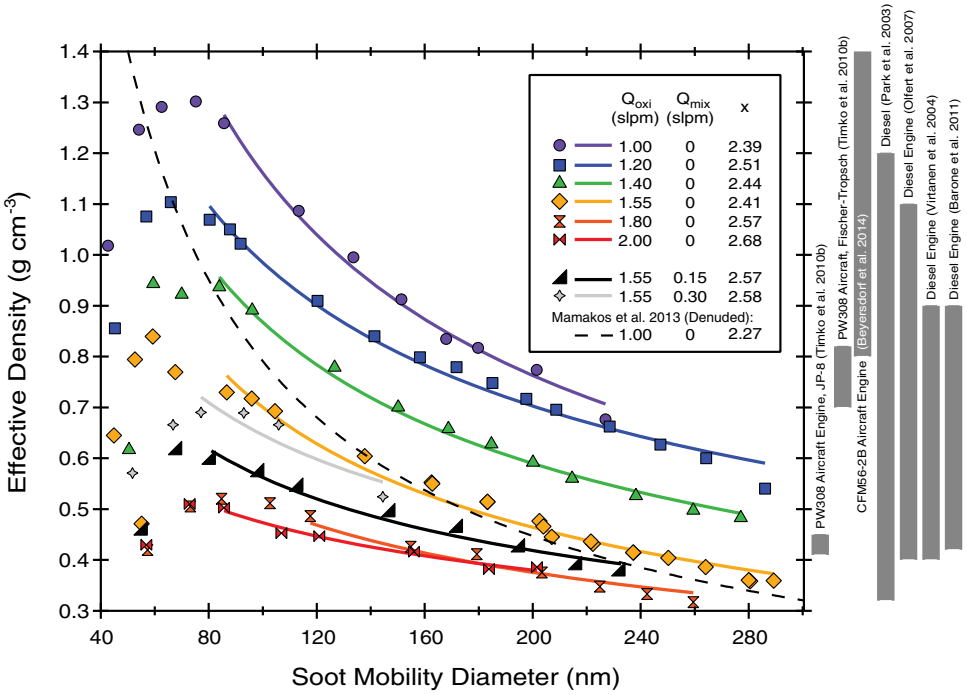

FIG. 9. Effective density of Mini-CAST soot. Shown for comparison are the density ranges reported for combustion soot in the literature.

by integrating the number size distribution. Over the period of February–June 2012, the soot number concentration varies by approximately two-fold, while the soot modal diameter varies by less than 10%. Greater variability is observed at high Q_{oxi}, where particle size and concentration are lowest, owing to increased soot oxidation in the very fuel-lean flame.

Petzold et al. (2009) identified the Mini-CAST as a "good candidate for a portable soot source," based on reproducibility of soot concentration and mass at five different flame conditions ($\phi < 1$) as measured by a CPC and a multi-angle absorption photometer, respectively. Schlatter (2002) evaluated an earlier CAST model and found short-term variability of the soot concentration output of ~4% over 10 min periods. Marsh et al. (2011) found that the Mini-CAST (Model 6201) output varied by 10% and 20% for soot number and mass concentrations during two experiments on consecutive days, respectively.

4.6. Comparison to Aircraft and Diesel Soot Sources

The Mini-CAST burner offers the convenience and reliability of a portable soot source for verification of analytical instrumentation or performing fundamental studies on soot aging and other processes; however, its true utility depends on the Mini-CAST soot having properties that are similar to soot emitted by real-world sources such as on- and off-road diesel engines and aircraft turbofan engines. The detailed characterization presented in the previous sections represents a step toward this goal by providing the first, comprehensive characterization of the Mini-CAST over a wide range of operating conditions. The burner soot can be broadly classified into three regimes as shown in Table 1: high-OC soot produced under both fuel-rich and fuel-lean conditions and low-OC soot produced only under fuel-lean conditions. Properties for each regime are summarized in Table 1, along with typical values reported in the literature for aircraft engine and diesel engine emissions. The emissions values reported here are presented for comparison purposes only and are not intended to reflect a critical review of the literature regarding past measurements. As such, the studies represent a variety of different sampling conditions and engine types.

The mode of the number size distribution of aircraft soot is typically much smaller than that for diesel engine exhaust, due to the much higher engine operating temperatures and pressures. Reported mode diameters range from 10–60 nm and 20–120 nm, respectively; although, the aircraft soot mode is most commonly observed around 30 nm, while the diesel engine soot mode is most commonly found around 70–90 nm (with a small nucleation mode <30 nm sometimes reported). Both of these size ranges overlap with the Mini-CAST size range, although the low-OC Mini-CAST soot is much larger than typical aircraft soot.

Reported OC/TC ratios for aircraft and diesel emissions of 30%–90% and 30%–80%, respectively, indicate that it is reasonable to use higher-OC Mini-CAST soot as a surrogate for these emissions, as engines typically emit OC-rich soot at idle conditions after the exhaust is cooled. One potential solution for those

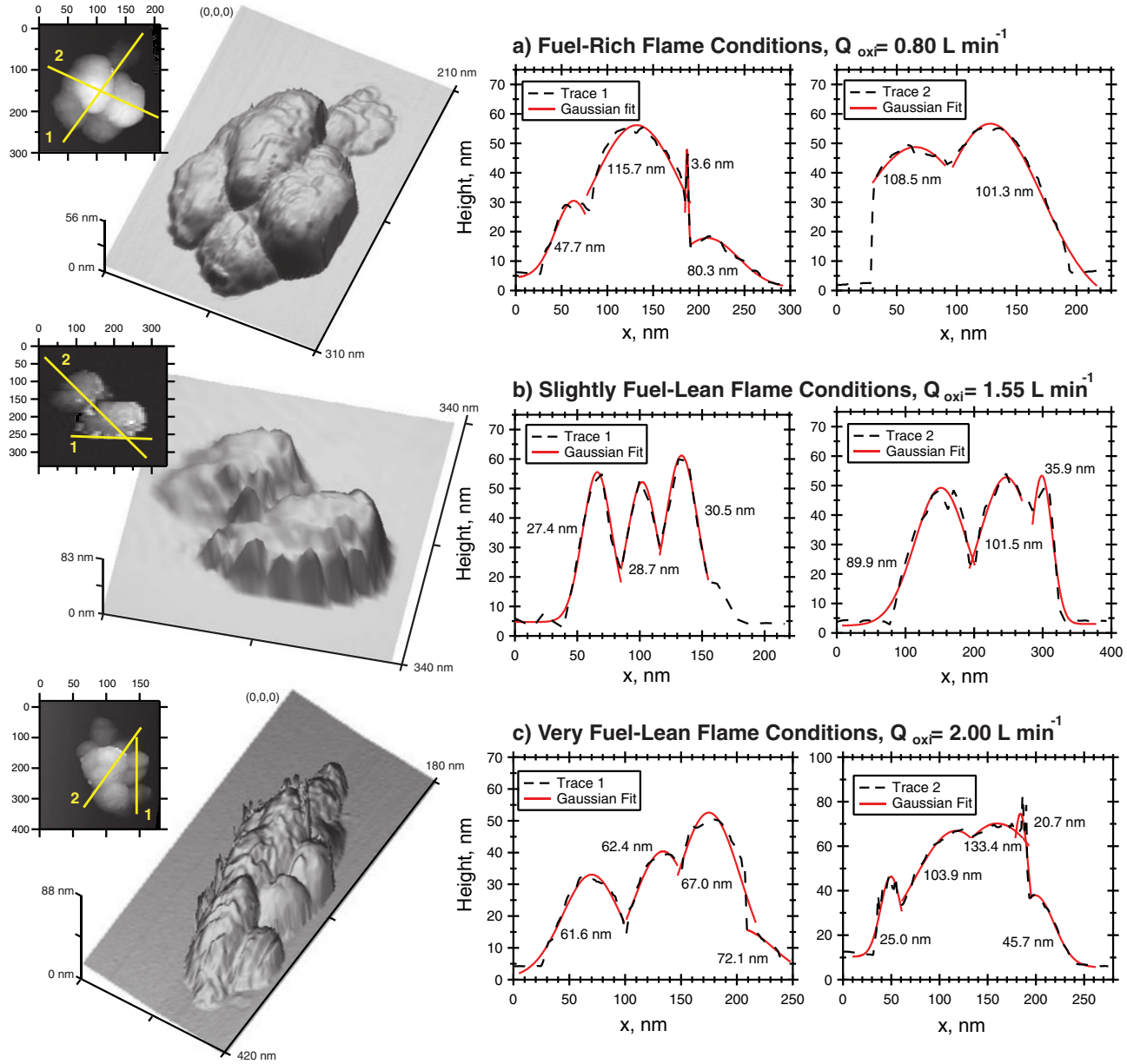

FIG. 10. Atomic force microscopy images of single, soot agglomerates at three different Mini-CAST conditions. Height profiles are shown to the right for two linear traces denoted by the lines in the top-down view insets. The dashed lines reflect the measured traces, while the solid lines are Gaussian fits to each clearly discernible peak. For each peak, the full Gaussian width at half maximum (FWHM) was computed and is reported beside each peak.

seeking to simulate low-OC, small-diameter soot characteristic of that from cruise aircraft is to employ a heated, catalytic stripper to remove some of the organic coating. This was explored in Figure 4a with moderate success, and it might be expected that a higher denuder temperature would remove even more coating. Tests where the flow through the denuder was reduced showed improved coating evaporation, but at the expense of increased coagulation and particle size (not shown). The number concentration of particles emitted by the Mini-CAST is comparable to concentrations measured from the engine sources; although, in many cases dilution will be required to bring the particle concentrations within the range of analytical instrumentation (typically $\leq 10^5$ cm^{-3}).

HR-ToF-AMS analysis of the soot coatings indicates a relatively low degree of oxygenation for both aircraft and diesel soots, as well as for the Mini-CAST soot, with O:C ratios ranging from ~0 to 0.25. This results in the soot acting as poor CCN with activated fractions of 0%–30% and $\kappa \sim 10^{-3}$. We note that this differs from the findings of Popovicheva et al. (2008), who found aircraft engine soot to be hygroscopic in the sense

TABLE 1
Summary of Mini-CAST soot properties and typical soot properties reported for aircraft and diesel engine combustion particles. Mini-CAST number concentrations have been corrected for the 172:1 (v/v) eductor dilution but not for coagulation in the sample lines

	Mini-CAST soot generator				
Property	Fuel-rich, high OC	Fuel-lean, low OC	Fuel-lean, high OC	Aircraft engine	Diesel engine
Q_{oxi}, L min^{-1}	0.6–1.1	1.1–1.8	1.8–2.2		
Q_{mix}, L min^{-1}	0.0	0.0	0.0		
Number mode diameter, nm	10–60	70–130	10–60	10–60[i,q]	20–120[c,o,s]
Number concentration, cm^{-3}	10^7–10^8	$10^7 - 5 \times 10^7$	10^6–10^7	10^{14}–10^{17}[†,g,h,j]	10^5–10^9 [s]
OC/TC fraction, %	50–90	30–50	50–90	30–90[r]	30–80[n,o]
Organic coating O:C ratio	0.05–0.08	0.08–0.15	0.15–0.25	0.1–0.2[p]	0.025–0.03[k,t]
Hygroscopicity (κ)	Not CCN	0	0–10^{-3}	$< 5 \times 10^{-3}$ [m,u]	0–10^{-2} [l]
Effective density, g cm^{-3}	0.8–1.3	0.45–1.1	0.3–0.5	0.3–0.9[e,f]	0.3–1.2[a,b,c,d]

[†]Computed assuming 2.5% CO_2 mixing ratio at the engine exhaust plane and 3160 ppm CO_2 (kg fuel)$^{-1}$, [a]Park et al. (2003), [b]Olfert et al. (2007), [c]Virtanen et al. (2004), [d]Barone et al. (2011), [e]Timko et al. (2010b), [f]Beyersdorf et al. (2014), [g]Herndon et al. (2005), [h]Anderson et al. (1998), [i]Lobo et al. (2007), [j]Timko et al. (2010a), [k]Aiken et al. (2008), [l]Tritscher et al. (2011), [m]Popovicheva et al. (2010), [n]Shah et al. (2004), [o]Kerminen et al. (1997), [p] Robinson (2011), [q]DeWitt et al. (2010), [r]Cheng et al. (2009), [s]Kittelson (1998), [t]Kroll et al. (2012), and [u]Petzold et al. (2005).

that many more monolayers of water could be absorbed on the engine soot versus the burner-generated soot.

5. SUMMARY AND CONCLUSIONS

The Miniature Combustion Aerosol Standard (Mini-CAST) soot generator is a portable and reliable source of combustion particles that can be used for instrument verification or process-based studies. Here, we present a comprehensive characterization of the microphysical, chemical, morphological, and hygroscopic properties of this soot, and show that the observed Mini-CAST soot properties overlap with the range of properties reported in the literature for real-world aircraft and diesel engine sources. Soot mode size, concentration, and OC fraction can be adjusted by varying the burner flow rates (Q_{oxi} and Q_{mix}), with the smallest particle size modes dominated by OC and the largest particle size modes consisting mainly of EC. Organic coatings present under fuel-rich flame conditions have a greater contribution from PAH and aromatic compounds, while more oxygenated, aliphatic compounds are present under fuel-lean conditions. These coatings drive the soot hygroscopicity, with none of the fuel-rich soot acting as CCN and a small fraction of the more oxygenated soot acting as CCN near the Kelvin activation limit. Effective density measurements and atomic force microscopy analysis show a spectrum of morphologies

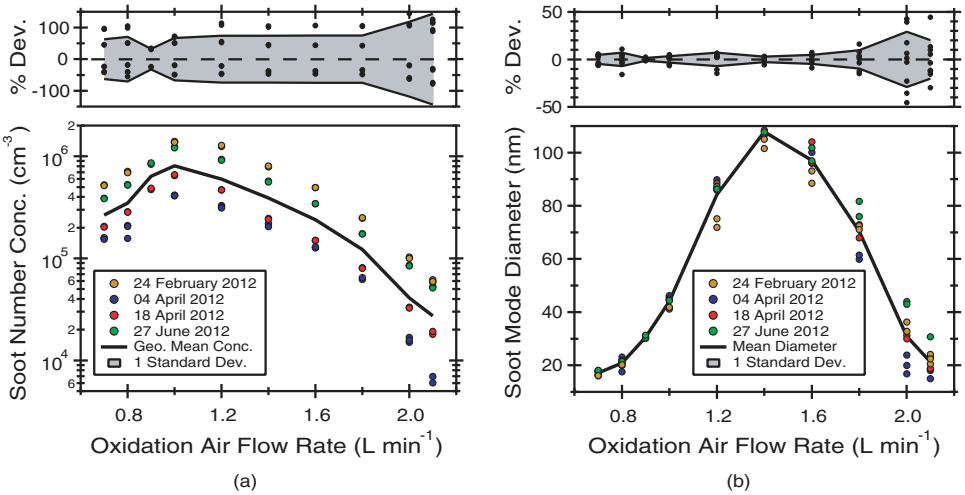

FIG. 11. (a) Size distribution mode and (b) number concentration reproducibility assessed over a period of months for varying Q_{oxi} and constant $Q_{mix} = 0.0$ L min^{-1}.

from spherical, OC-rich particles to more agglomerated, lower-density EC-rich particles.

Measurements of soot mode size and concentration conducted over a period of several months indicate that the burner output is stable to within <10% in terms of mode diameter and a factor of two in terms of concentration, where the high concentration variability may be due to a variety of factors such as soot accumulation in the sampling lines and metering valves or small changes in the fuel gas, nitrogen, or air composition associated with cylinder changes. Careful attention to and control of these factors may reduce this temporal variation.

ACKNOWLEDGMENTS

RHM acknowledges support from a NASA Postdoctoral Program Fellowship.

FUNDING

The authors thank the NASA Fundamental Aeronautics and Fixed Wing Programs for funding support. The CFD code was developed by A. Nenes (http://nenes.eas.gatech.edu/CFD).

SUPPLEMENTARY MATERIALS

Supplemental data for this article can be accessed on the publisher's website.

REFERENCES

Aiken, A. C., DeCarlo, P. F., and Jimenez, J. L. (2007). Elemental Analysis of Organic Species with Electron Ionization High-resolution Mass Spectrometry. *Anal. Chem.*, 79:8350–8358.

Aiken, A. C., DeCarlo, P. F., Kroll, J. H., Worsnop, D. R., Huffman, J. A., Docherty, K. S., Ulbrich, I. M., Mohr, C., Kimmel, J. R., Sueper, D., Sun, Y., Zhang, Q., Trimborn, A., Northway, M., Ziemann, P. J., Canagaratna, M. R., Onasch, T. B., Alfarra, M. R., Prevot, A. S., Dommen, J., Duplissy, J., Metzger, A., Baltensperger, U., and Jimenez, J. L. (2008). O/C and OM/OC Ratios of Primary, Secondary, and Ambient Organic Aerosols with High-resolution Time-of-flight Aerosol Mass Spectrometry. *Environ. Sci. Technol.*, 42:4478–4485.

Anderson, B. E., Cofer, W. R., Bagwell, D. R., Barrick, J. W., Hudgins, C. H., and Brunke, K. E. (1998). Airborne Observations of Aircraft Aerosol Emissions I: Total Nonvolatile Particle Emission Indices. *Geophys. Res. Lett.*, 25:1689–1692.

Barone, T. L., Lall, A. A., Storey, J. M. E., Mulholland, G. W., Prikhodko, V. Y., Fankland, J. H., Parks, J. E., and Zachariah, M. R. (2011). Size-resolved Density Measurements of Particle Emissions from an Advanced Combustion Diesel Engine: Effect of Aggregate Morphology. *Energy Fuels*, 25:1978–1988.

Barthazy, E., Stetzer, O., Derungs, C., Saathoff, H., and Lohmann, U. (2006). Water Uptake of Soot Particles Emitted from a Jing-CAST Soot Generator, in *Proceedings of the 12th Conference on Cloud Physics, American Meteorological Society Annual Meeting*.

Barthazy, E., Stetzer, O., Derungs, C., Wahlen, S., and Lohmann, U. (2007). Characterization of a Propane Soot Generator, in *Nucleation and Atmospheric Aerosols*, C. D. O'Dowd and P. E. Wagner, eds, Springer, The Netherlands, pp. 834–839.

Baumgardner, D., Popovicheva, O., Allan, J., Bernardoni, V., Cao, J., Cavalli, F., Cozic, J., Diapouli, E., Eleftheriadis, K., Genberg, P. J., Gonzalez, C., Gysel, M., John, A., Kirchstetter, T. W., Kuhlbusch, T. A. J., Laborde, M., Lack, D., Müller, T., Niessner, R., Petzold, A., Piazzalunga, A., Putaud, J. P., Schwarz, J., Sheridan, P., Subramanian, R., Swietlicki, E., Valli, G., Vecchi, R., and Viana, M. (2012). Soot Reference Materials for Instrument Calibration and Intercomparisons: A Workshop Summary with Recommendations. *Atmos. Meas. Tech.*, 5:1869–1887.

Beyersdorf, A. J., Timko, M. T., Ziemba, L. D., Bulzan, D., Corporan, E., Herndon, S. C., Howard, R., Miake-Lye, R., Thornhill, K. L., Winstead, E., Wey, C., Yu, Z., and Anderson, B. E. (2014). Reductions in Aircraft Particulate Emissions Due to the use of Fischer-Tropsch Fuels. *Atmos. Chem. Phys.*, 14:11–24.

Bond, T. C., Doherty, S. J., Fahey, D. W., Forster, P. M., Berntsen, T., DeAngelo, B. J., Flanner, M. G., Ghan, S., Kärcher, B., Koch, D., Kinne, S., Kondo, Y., Quinn, P. K., Sarofim, M. C., Schultz, M. G., Schulz, M., Venkataraman, C., Zhang, H., Zhang, S., Bellouin, N., Guttikunda, S. K., Hopke, P. K., Jacobson, M. Z., Kaiser, J. W., Klimont, Z., Lohmann, U., Schwarz, J. P., Shindell, D., Storelvmo, T., Warren, S. G., and Zender, C. S. (2013). Bounding the Role of Black Carbon in the Climate System: A Scientific Assessment. *J. Geophys. Res.*, 118(11):5380–5552.

Cheng, M.-D., Corporan, E., DeWitt, M. J., and Landgraf, B. (2009). Emissions of Volatile Particulate Components from Turboshaft Engines Operated with JP-8 and Fischer-Tropsch Fuels. *Aerosol Air Qual. Res.*, 9:237–256.

Crawford, I., Möhler, O., Schnaiter, M., Saathoff, H., Liu, D., McMeeking, G., Linke, C., Flynn, M., Bower, K. N., Connolly, P. J., Gallagher, M. W., and Coe, H. (2011). Studies of Propane Flame Soot Acting as Heterogeneous Ice Nuclei in Conjunction with Single Particle Soot Photometer Measurements. *Atmos. Chem. Phys.*, 11:9549–9561.

Cross, E. S., Onasch, T. B., Ahern, A., Wrobel, W., Slowik, J. G., Olfert, J., Lack, D. A., Massoli, P., Cappa, C. D., Schwarz, J. P., Spackman, J. R., Fahey, D. W., Sedlacek, A., Trimborn, A., Jayne, J. T., Freedman, A., Williams, L. R., Ng, N. L., Mazzoleni, C., Dubey, M., Brem, B., Kok, G., Subramanian, R., Freitag, S., Clarke, A., Thornhill, D., Marr, L. C., Kolb, C. E., Worsnop, D. R., and Davidovits, P. (2010). Soot Particle Studies – Instrument Intercomparison – Project Overview. *Aerosol Sci. Technol.*, 44:592–611.

DeCarlo, P. F., Kimmel, J. R., Trimborn, A., Northway, M. J., Jayne, J. T., Aiken, A. C., Gonin, M., Fuhrer, K., Horvath, T., Docherty, K. S., Worsnop, D. R., and Jimenez, J. L. (2006). Field-deployable, High-resolution, Time-of-flight Aerosol Mass Spectrometer. *Anal. Chem.*, 78:8281–8289.

DeWitt, M. J., Klingshirn, C. D., and Anneken, D. (2010). Alternative Fuels Tests on a C-17 Aircraft: Emissions Characteristics – Interim Report. Technical Report AFRL-RZ-WP-TR-2011-2004, Air Force Research Laboratory, Propulsion Directorate, Wright-Patterson Air Force Base.

Friedman, B., Kulkarni, G., Baeránek, J., Zelenyuk, A., Thornton, J. A., and Cziczo, D. J. (2011). Ice Nucleation and Droplet Formation by Bare and Coated Soot Particles. *J. Geophys. Res.*, 116:D17203.

Henning, S., Ziese, M., Kiselev, A., Saathoff, H., Möhler, O., Mentel, T. F., Buchholz, A., Spindler, C., Michaud, V., Monier, M., Sellegri, K., and Stratmann, F. (2012). Hygroscopic Growth and Droplet Activation of Soot Particles: Uncoated, Succinic or Sulfuric Acid Coated. *Atmos. Chem. Phys.*, 12:4525–4537.

Herndon, S. C., Onasch, T. B., Frank, B. P., Marr, L. C., Jayne, J. T., Canagaratna, M. R., Grygas, J., Lanni, T., Anderson, B. E., Worsnop, D., and Miake-Lye, R. C. (2005). Particulate Emissions from In-use Commercial Aircraft. *Aerosol Sci. Technol.*, 39:799–809.

Jacobson, M. Z. (2001). Strong Radiative Heating Due to the Mixing State of Black Carbon in Atmospheric Aerosols. *Nature*, 409:695–697.

Janssen, N. A. H., Hoek, G., Simic-Lawson, M., Fischer, P., van Bree, L., ten Brink, H., Keuken, M., Atkinson, R. W., Anderson, H. R., Brunekreef, B., and Cassee, F. R. (2011). Black Carbon as an Additional Indicator of the Adverse Health Effects of Airborne Particles Compared with PM_{10} and $PM_{2.5}$. *Environ. Health Perspect.*, 119:1691–1699.

Jayne, J. T., Leard, D. C., Zhang, X., Davidovits, P., Smith, K. A., Kolb, C. A., and Worsnop, D. R. (2000). Development of an Aerosol Mass Spectrometer for Size and Composition Analysis of Submicron Particles. *Aerosol Sci. Technol.*, 33:49–70.

Jing, L. (1999). Standard Combustion Aerosol Generator (SCAG) for Calibration Purposes, in *3rd ETH Workshop on Nanoparticle Measurement*, CD-ROM.

Kerminen, V.-M., Mäkelä, T. E., Ojanen, C. H., Hillamo, R. E., Vilhunen, J. K., Rantanen, L., Havers, N., Bohlen, A. V., and Klockow, D. (1997). Characterization of the Particulate Phase in the Exhaust from a Diesel Car. *Environ. Sci. Technol*., 31:1883–1889.

Kittelson, D. B. (1998). Engines and Nanoparticles: A Review. *J. Aerosol Sci*., 29:575–588.

Kroll, J. H., Smith, J. D., Worsnop, D. R., and Wilson, K. R. (2012). Characterization of Lightly Oxidized Organic Aerosol Formed from the Photochemical Aging of Diesel Exhaust Particles. *Environ. Chem*., 9: 211–220.

Kumfer, B., and Kennedy, I. (2007). The Role of Soot in the Health Effects of Inhaled Airborne Particles, in *Combustion Generated Fine Carbonaceous Particles*, B. H., A. D'Anna, A. F. Sarofim, and H. Wang, eds., KIT Scientific Publishing, Karlsruhe, Germany, pp. 1–15.

Lall, A. A., and Friedlander, S. K. (2006). On-line Measurement of Ultrafine Aggregate Surface Area and Volume Distributions by Electrical Mobility Analysis: I. Theroetical Analysis. *Aerosol Sci*., 37:260–271.

Lance, S., Medina, J., Smith, J. N., and Nenes, A. (2006). Mapping the Operation of the DMT Continuous-flow CCN Counter. *Aerosol Sci. Technol*., 40:242–254.

Lobo, P., Hagen, D. E., Whitefield, P. D., and Alofs, D. J. (2007). Physical Characterization of Aerosol Emissions from a Commercial Gas Turbine Engine. *J. Propul. Power*, 23:919–929.

Mamakos, A., Khalek, I., Giannelli, R., and Spears, M. (2013). Characterization of Combustion Aerosol Produced by a Mini-CAST and Treated in a Catalytic Stripper. *Aerosol Sci. Technol*., 47:927–936.

Marsh, R., Crayford, A., Petzold, A., Johnson, M., Williams, P., Ibrahim, A., Kay, P., Morris, S., Delhaye, D., Lottin, D., Vancassel, X., Raper, D., Christie, S., Bennett, M., Miller, M., Sevcenco, Y., Rojo, C., Coe, H., and Bowen, P. (2011). Studying, Sampling and Measurement of Aircraft Particulate Emissions II (SAMPLE II) – Final Report. Technical Report EASA.2009/OP18, European Aviation Safety Agency.

Möhler, O., Linke, C., Saathoff, H., Schnaiter, M., Wagner, R., Mangold, A., Krämer, M., and Schurath, U. (2005). Ice Nucleation on Flame Soot Aerosol of Different Organic Carbon Content. *Meteorol. Z*., 14(4):477–484.

Moore, R. H., Nenes, A., and Medina, J. (2010). Scanning Mobility CCN Analysis – A Method for Fast Measurements of Size-resolved CCN Distributions and Activation Kinetics. *Aerosol Sci. Technol*., 44:861–871.

Olfert, J. S., Symonds, J. P. R., and Collings, N. (2007). The Effective Density and Fractal Dimension of Particles Emitted from a Light-duty Diesel Vehicle with a Diesel Oxidation Catalyst. *Aerosol Sci*., 38:69–82.

Park, K., Cao, F., Kittelson, D. B., and McMurry, P. H. (2003). Relationship between Particle Mass and Mobility for Diesel Exhaust Particles. *Environ. Sci. Technol*., 37:577–583.

Petters, M. D., and Kreidenweis, S. M. (2007). A Single Parameter Representation of Hygroscopic Growth and Cloud Condensation Nucleus Activity. *Atmos. Chem. Phys*., 7:1961–1971.

Petzold, A., Gysel, M., Vancassel, X., Hitzenberger, R., Puxbaum, H., Vrochticky, S., Weingartner, E., Baltensperger, U., and Mirabel, P. (2005). On the Effects of Organic Matter and Sulphur-containing Compounds on the CCN Activation of Combustion Particles. *Atmos. Chem. Phys*., 5:3187–3203.

Petzold, A., Marsh, R., Johnson, M., Miller, M., Sevcenco, Y., Delhaye, D., Vancassel, X., Ibrahim, A., Veira, A., Williams, P., Bauer, H., Crayford, A., Morris, S., Kay, P., Bowen, P., Bachalo, W. D., and Raper, D. (2009). Study on Sampling and Measurement of Aircraft Particulate Emissions SAMPLE – Final report. Technical Report No. EASA.2008/OP13, European Aviation Safety Agency (EASA).

Petzold, A., Ogren, J. A., Fiebig, M., Laj, P., Li, S.-M., Baltensperger, U., Holzer-Popp, T., Kinne, S., Pappalardo, G., Sugimoto, N., Wehrli, C., Wiedensohler, A., and Zhang, X.-Y. (2013). Recommendations for Reporting "Black Carbon" Measurements. *Atmos. Chem. Phys*., 13:8365–8379.

Popovicheva, O. B., Kireeva, E. D., Timofeev, M. A., Shonija, N. K., and Mogil'nikov, V. P. (2010). Cabonaeous Aerosols of Aviation and Shipping Emissions. *Izv. Atmos. Ocean. Phys*., 46:368–375.

Popovicheva, O. B., Persiantseva, N. M., Tishkova, V., Shonija, N. K., and Zubareva, N. A. (2008). Quantification of Water Uptake by Soot Particles. *Environ. Res. Lett*., 3:025009.

Roberts, G. C., and Nenes, A. (2005). A Continuous-flow Streamwise Thermal-gradient CCN Chamber for Atmospheric Measurements. *Aerosol Sci. Technol*., 39:206–221.

Robinson, A. L. (2011). Measurement and Modeling of Volatile Particle Emissions from Military Aircraft – Final Report. Technical Report, SERDP Project WP-1626, SERDP.

Schlatter, J. (2002). Application of CAST for Comparison of Instruments, in *Proceedings of the 6th ETH Conference on Nanoparticle Measurement*, CD-ROM.

Schmidt-Ott, A., Baltensperger, U., Gäggeler, H. W., and Jost, D. T. (1990). Scaling Behaviour of Physical Parameters Describing Agglomerates. *J. Aerosol Sci*., 21:711–717.

Schnaiter, M., Gimmler, M., Llamas, I., Linke, C., Jäger, C., and Mutschke, H. (2006). Strong Spectral Dependence of Light Absorption by Organic Carbon Particles Formed by Propane Combustion. *Atmos. Chem. Phys*., 6:2981–2990.

Shah, S. D., Cocker, D. R., III, Miller, J. W., and Norbeck, J. M. (2004). Emissions Rates of Particulate Matter and Elemental and Organic Carbon from In-use Diesel Engines. *Environ. Sci. Technol*., 38:2544–2550.

Sorensen, C. M. (2011). The Mobility of Fractal Aggregates: A Review. *Aerosol Sci. Technol*., 45:765–779.

Subramanian, R., Khlystov, A. Y., and Robinson, A. L. (2006). Effect of Peak Inert-mode Temperature on Elemental Carbon Measured using Thermal-optical Analysis. *Aerosol Sci. Technol*., 40:763–780.

Swanson, J., and Kittelson, D. (2010). Evaluation of Thermal Denuder and Catalytic Stripper Methods for Solid Particle Measurements. *J. Aerosol Sci*., 41:1113–1122.

Timko, M. T., Onasch, T. B., Northway, M. J., Jayne, J. T., Canagaratna, M. R., Herndon, S. C., Wood, E. C., Miake-Lye, R. C., and Knighton, W. B. (2010a). Gas Turbine Engine Emissions – Part II: Chemical Properties of Particulate Matter. *J. Eng. Gas Turbines Power*, 132:061505.

Timko, M. T., Yu, Z., Onasch, T. B., Wong, H.-W., Miake-Lye, R. C., Beyersdorf, A. J., Anderson, B. E., Thornhill, K. L., Winstead, E. L., Corporan, E., DeWitt, M. J., Klingshirn, C. D., Wey, C., Tacina, K., Liscinsky, D. S., Howard, R., and Bhargava, A. (2010b). Particulate Emissions of Gas Turbine Engine Combustion of a Fischer-Tropsch Synthetic Fuel. *Energy Fuels*, 24:5883–5896.

Tritscher, T., Jurányi, Z., Martin, M., Chirico, R., Gysel, M., Heringa, M. F., DeCarlo, P. F., Sierau, B., Prévôt, A. S. H., Weingartner, E., and Baltensperger, U. (2011). Changes in Hygroscopicity and Morphology During Ageing of Diesel Soot. *Environ. Res. Lett*., 6:034026.

Virtanen, A. K. K., Ristimäki, J. M., Vaaraslhti, K. M., and Keskinen, J. (2004). Effect of Engine Load on Diesel Soot Particles. *Environ. Sci. Technol*., 38:2551–2556.

Wall, S. (1996). Improved Methods for PAH Combustion Source Sampling. Technical Report, Contract A932–098, California Air Resources Board.

Warnatz, J., Mass, U., and Dibble, R. W. (2001). *Combustion: Physical and Chemical Fundamentals, Modeling and Simulation, Experiments, Pollutant Formation,* 3rd ed., Springer, New York, 229 p.

Supplemental Information for Mapping the Operation of the Miniature Combustion Aerosol Standard (Mini-CAST) Soot Generator

Richard H. Moore

NASA Postdoctoral Program, NASA Langley Research Center

Luke D. Ziemba

NASA Langley Research Center

Dabrina Dutcher

Bucknell University

Andreas J. Beyersdorf

NASA Langley Research Center

Kevin Chan

NASA Langley Research Center

Suzanne Crumeyrolle

NASA Postdoctoral Program, NASA Langley Research Center

Timothy M. Raymond

Bucknell University

Kenneth L. Thornhill

NASA Langley Research Center

Edward L. Winstead

NASA Langley Research Center

Bruce E. Anderson

NASA Langley Research Center

S1. Simplified Numerical Burner Simulation

Numerically simulating soot formation in diffusion flames is a complex process involving tens to hundreds of different chemical reactions that occur within the flame, and a number of models with detailed chemistry have been developed toward this end [e.g., *Smooke et al.*, 1999, 2005]. Here, we apply a vastly-simplified, mixing-fraction-based model in order to qualitatively examine soot formation within the Mini-CAST flame for one set of operational conditions. A conserved-scalar approach is employed, where a computational fluid dynamics model (online at http://nenes.eas.gatech.edu/CFD/) [*Nenes et al.*, 2001] is used to determine the spatial distribution of fuel mixture fraction, f, where f=1 at the

fuel flow entrance plane and f=0 at the oxidant entrance plane. *Turns* [1996] describe an analytical solution for the temperature profile in terms of mixture fraction for a laminar, axisymmetric diffusion flame burning in a quiescent oxidizer reservoir. This method invokes a number of assumptions including the flame-sheet approximation, Fickian diffusion, unit Lewis number, and neglects the effects of radiation heat transfer, axial diffusion, and buoyancy. We employ this solution, here, to approximate the temperature distribution in the Mini-CAST flame, but apply a scaling factor, ϵ, of 0.7 to account for radiative heat loss not captured by these simplified thermodynamics [*Sivathanu and Faeth*, 1990]:

$$T(f) = \begin{cases} (1-f)\left(\frac{f_{st}}{1-f_{st}}\epsilon\frac{\Delta h_c}{c_p}\right) + T_{oxi} & \text{if } f_{st} < f \leq 1 \\ f\epsilon\frac{\Delta h_c}{c_p} + T_{oxi} & \text{if } 0 \leq f \leq f_{st} \end{cases} \quad \text{(S1)}$$

where f_{st} is the stoichiometric mixture fraction (0.15 for propane and air), h_c is the enthalpy of combustion for propane, c_p is the heat capacity of air, and T_{oxi} is the entrance temperature of the fuel and air streams. The simulated temperature distribution for a Mini-CAST flame with $Q_{\text{fuel}} = 0.06$ L min^{-1}, $Q_{\text{oxi}} = 1.55$ L min^{-1}, and $Q_{\text{mix}} = 0$ L min^{-1} is shown in Figure 1a, where the upper portion of the flame is cropped to indicate the quench height.

Following *Lautenberger et al.* [2005], soot formation and oxidation zones are computed in terms of the localized flame mixture fraction and temperature. Soot formation occurs over a narrow range of temperatures ($1375 < T < 1825$ K), where the fuel:oxidant ratio is slightly richer than stoichiometric ($0.158 < f < 0.323$), while soot oxidation is controlled by the production of OH$^\bullet$, which is governed by the availability of oxygen on the fuel-lean side of the flame sheet ($0.08 < f < 0.15$) and temperatures high enough for oxygen and H$^\bullet$ to form OH$^\bullet$ ($T > 1375$ K) [*Lautenberger et al.*, 2005]. Using this simple, analytical soot model, the soot formation and oxidation zones within the Mini-CAST burner are computed to be those shown in Figure 1b. It can be seen that while the soot formation zone extends from the base of the flame to the quench height, the soot formed near the center of the flame never encounters the oxidation region, which allows high concentrations of soot to escape. As discussed in the main article, adjustment of the gas flow rates into the combustion chamber changes the extent of the soot formation and oxidation zones, which alters the soot concentration and properties.

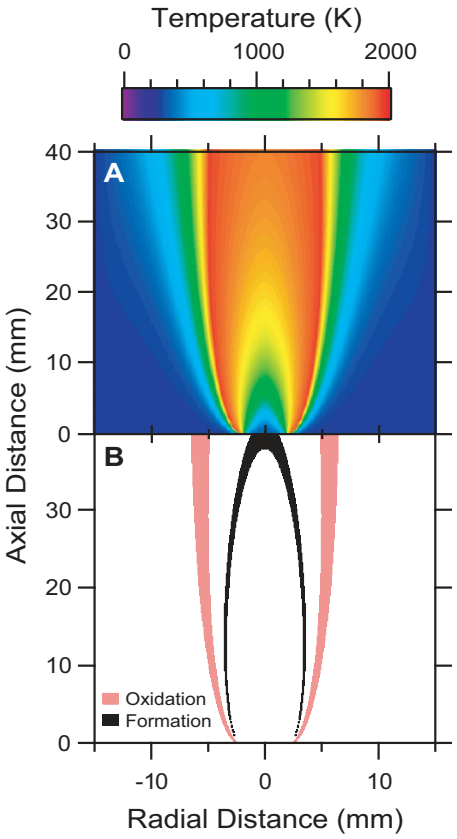

Figure S1: Simulated (A) flame temperature and (B) soot formation and oxidation regions within the Mini-CAST burner for $Q_{oxi} = 1.55$ L min^{-1} and $Q_{mix} = 0.00$ L min^{-1}.

S2. Comparison of Organic Carbon Fraction Data to Reported Literature Values

Previous studies examining the organic carbon (OC) fraction of soot total carbon (TC) have reported these values in terms of the overall flame C:O ratio [e.g., *Schnaiter et al.*, 2006; *Crawford et al.*, 2011; *Mamakos et al.*, 2013]. Consequently, we report the data from this study in this manner in Figure 2 for comparison. As discussed in the main text, the flame C:O ratio does not incorporate changes in the flame soot characteristics resulting from including inert mixing N_2 in the fuel flow, which is shown to both decrease the soot mode size and increase the OC/TC ratio. Past studies have also focused primarily on fuel-rich flames, which suggest that OC/TC varies monotonically with flame C:O ratio; however, the results of the present study indicates that OC/TC increases for soot produced under very fuel-lean

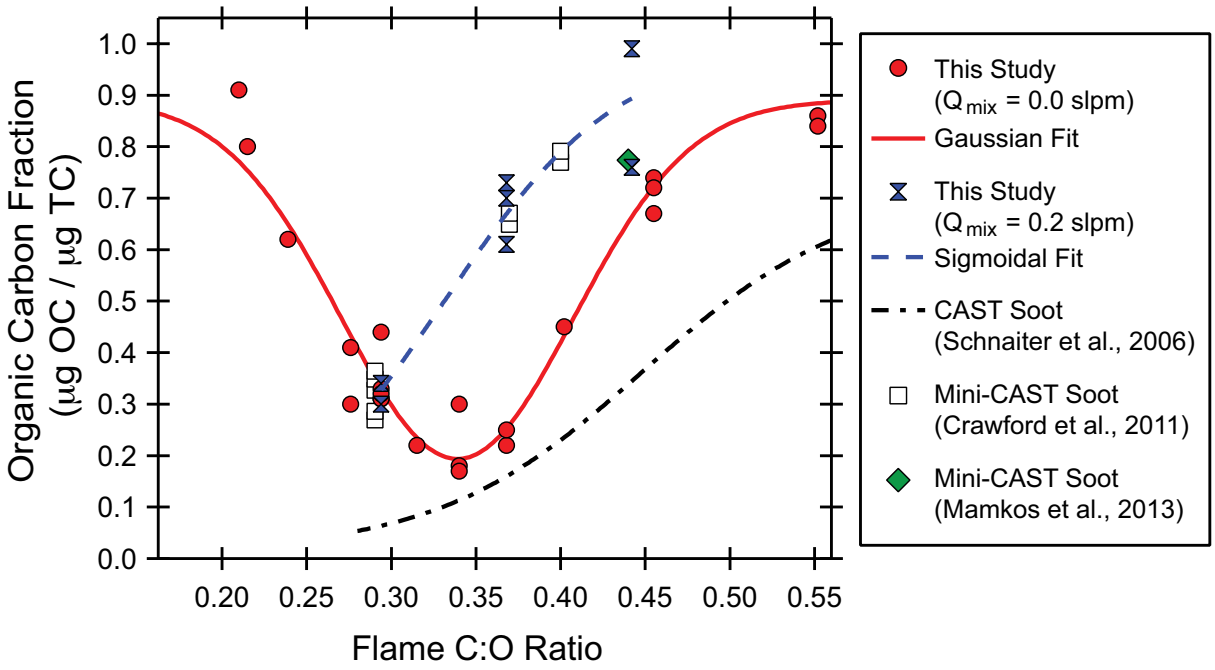

Figure S2: Organic carbon fraction as a function of overall flame O:C ratio. Data shown are for $Q_{\mathrm{mix}} = 0.0$ and 0.2 L min^{-1}, and are compared to OC fractions from *Schnaiter et al.* [2006], *Crawford et al.* [2011], and *Mamakos et al.* [2013]. Fit lines are included to guide the eye.

flame conditions (Figure 2). A simple way to account for this complex dependence is to parameterize OC/TC in terms of soot mode size (Figure 4a in the main text).

References

Crawford, I., O. Möhler, M. Schnaiter, H. Saathoff, D. Liu, G. McMeeking, C. Linke, M. Flynn, K. N. Bower, P. J. Connolly, M. W. Gallagher, and H. Coe, Studies of propane flame soot acting as heterogeneous ice nuclei in conjunction with single particle soot photometer measurements, *Atmospheric Chemistry and Physics*, *11*, 9549–9561, doi:10.5194/acp-11-9549-2011, 2011.

Lautenberger, C. W., J. L. de Ris, N. A. Dembsey, J. R. Barnett, and H. R. Baum, A simplified model for soot formation and oxidation in CFD simulation of non-premixed hydrocarbon flames, *Fire Safety Journal*, *40*, 141–176, doi:10.1016/j.firesaf.2004.10.002, 2005.

Mamakos, A., I. Khalek, R. Giannelli, and M. Spears, Characterization of combustion aerosol produced by a Mini-CAST and treated in a catalytic stripper, *Aerosol Science and Technology*, *47*, 927–936, doi:10.1080/02786826.2013.802762, 2013.

Nenes, A., P. Y. Chuang, R. C. Flagan, and J. H. Seinfeld, A theoretical analysis of cloud condensation nucleus (CCN) instruments, *Journal of Geophysical Research*, *106*, 3449–3474, doi:10.1029/2000JD900614, 2001.

Schnaiter, M., M. Gimmler, I. Llamas, C. Linke, C. Jäger, and H. Mutschke, Strong spectral dependence of light absorption by organic carbon particles formed by propane combustion, *Atmospheric Chemistry and Physics*, *6*, 2981–2990, doi:10.5194/acp-6-2981-2006, 2006.

Sivathanu, Y. R., and G. M. Faeth, Temperature / soot volume fraction correlations in the fuel-rich region of buoyant turbulent diffusion flames, *Combustion and Flame*, *81*, 150–165, 1990.

Smooke, M. D., C. S. McEnally, L. D. Pfefferle, R. J. Hall, and M. B. Colket, Computational and experimental study of soot formation in a coflow, laminar diffusion flame, *Combustion and Flame*, *117*, 117–139, doi:10.1016/S0010-2180(98)00096-0, 1999.

Smooke, M. D., M. B. Long, B. C. Connelly, M. B. Colket, and R. J. Hall, Soot formation in laminar diffusion flames, *Combustion and Flame*, *143*, 613–628, doi:10.1016/j.combustflame.2005.08.028, 2005.

Turns, S. R., *An Introduction to Combustion: Concepts and Applications*, McGraw-Hill, 1996.

R. Moore, NASA Langley Research Center, Hampton, VA 30332 (e-mail: richard.h.moore@nasa.gov)

Received N/A; revised N/A; accepted N/A.